Finite-temperature properties of $(Ba,Sr)TiO_3$ systems from atomistic simulations

Laura Walizer, Sergey Lisenkov, and L. Bellaiche
Physics Department, University of Arkansas, Fayetteville, Arkansas 72701, USA
(Received 19 January 2006; published 11 April 2006)

An effective Hamiltonian approach is developed to mimic finite-temperature properties of $(Ba_xSr_{1-x})TiO_3$ perovskite systems. It is found that this atomistic approach is overall quite accurate to qualitatively *and* quantitatively reproduce the experimental composition-temperature phase diagram of the *disordered solid solutions* (especially, for compositions x larger than 25%), when allowing one single parameter to deviate from its first-principles-derived value. Interestingly, such approach also yields predictions that are in good agreement with direct first-principles calculations for $BaTiO_3/SrTiO_3$ *superlattices*. The proposed approach is thus promising to investigate phenomena in any perovskite system made of Ba, Sr, Ti, and O atoms, independently of the overall composition and atomic arrangement.

DOI: 10.1103/PhysRevB.73.144105 PACS number(s): 77.84.Dy, 81.30.Bx, 77.80.Bh, 31.15.Ar

I. INTRODUCTION

Ferroelectric perovskite $(A'A'')BO_3$ [or $A(B'B'')O_3$] alloys are of growing importance for a variety of device applications[1,2] either when grown as solid solutions or in the form of $A'BO_3/A''BO_3$ (or $AB'O_3/AB''O_3$) superlattices. Such systems are also of large fundamental interest, mostly in order to reveal the microscopic effects responsible for their properties. A deep knowledge of ferroelectric alloys at an atomistic level has the potential to result in original and/or enhanced macroscopic properties. Accurate atomistic simulations are thus needed to understand the properties of perovskite alloys in general, and to guide the discovery of "wunderbar" materials, in particular. Within the last six years, three different kinds of atomistic simulations have been developed and used for perovskite alloys. One approach is the shell model that has been applied to disordered $(Ba_xSr_{1-x})TiO_3$ (BST) and $K(Ta_{1-x}Nb_x)O_3$ solid solutions as well as to $KTaO_3/KNbO_3$ superlattices.[3–6] In particular, the shell model qualitatively reproduces the experimental composition-temperature phase diagram of BST. However, it remains unknown if such an approach can also yield subtle alloy phenomena, such as the existence of the low-temperature monoclinic phase discovered in the phase diagram of $Pb(Zr_{1-x}Ti_x)O_3$ alloys for a narrow range of composition.[7] On the other hand, it has been shown that such unusual low-symmetry phase can be very well reproduced by another atomistic technique, namely the bond-valence model.[8] However, we are not aware of any study demonstrating that this latter model can mimic well superlattices as well as properties of ferroelectric alloys at intermediate or high temperatures (i.e., not only at low temperatures). Similarly, there is (at least) one limitation for the third kind of atomistic simulations, the alloy effective Hamiltonian method, which has been rather successful for describing properties of Pb-based systems. The limitation of this method is that any alloy effective Hamiltonian scheme developed so far is only technically applicable to a single composition or for a narrow compositional range around a specific concentration.[9–15] As a result, this prevents, e.g., the investigation of the *whole* composition-temperature phase diagram of disordered alloys, unless one develops a large number of effective Hamiltonians—each corresponding to a different overall composition.

The aim of the paper is to show that it is possible to develop a single alloy effective Hamiltonian method that can predict finite-temperature properties of solid solutions for the whole composition range as well as properties of superlattices having different overall concentrations. Here, we focus on perovskite systems made of Ba, Sr, Ti, and O atoms because of (1) the technological importance of BST solid solutions,[16] and (2) the numerous experimental and direct first-principles data that are already available in the literature for such systems (see, e.g., Refs. 3 and 17–19 and references therein), and that we can compare them to check the accuracy of our model.

This paper is organized as follows. Section II describes in detail the presently proposed effective Hamiltonian scheme. In Sec. III, we show and discuss the predictions for disordered BST solid solutions and $BaTiO_3/SrTiO_3$ superlattices obtained by this scheme. Finally, we present our conclusions in Sec. IV.

II. METHODS

Our scheme is based on the construction of an alloy effective Hamiltonian from first-principles calculations, with the total energy E being written as a sum of two different main terms

$$E(\{\mathbf{u}_i\},\eta_H,\{\eta_I\},\{\sigma_j\},\{\eta_{loc}\}) = E_{\text{ave}}(\{\mathbf{u}_i\},\eta_H,\{\eta_I\}) + E_{\text{loc}}(\{\mathbf{u}_i\},\{\eta_I\},\{\sigma_j\},\{\eta_{loc}\}), \quad (1)$$

where E_{ave}, as in Refs. 9–13, is the total energy associated with the hypothetical *simple* $\langle A\rangle BO_3$ system resulting from the use of the virtual crystal approximation[20–22] (VCA) to mimic $(Ba_{0.5}Sr_{0.5})TiO_3$; E_{loc} gathers terms associated with alloying effects going beyond the VCA approximation; $\mathbf{u}_i$ is the local soft mode (which is centered on B atoms) in unit cell i; η_H and $\{\eta_I\}$ are the *homogeneous* and *inhomogeneous* strain tensor[23] associated with the virtual $\langle Ba_{0.5}Sr_{0.5}\rangle TiO_3$ system, respectively; $\{\sigma_j\}$ characterizes the atomic configuration, that is, $\sigma_j=+1$ or -1 corresponds to the presence of a Ba or Sr atom, respectively, at the A-lattice site j of the

$(Ba_xSr_{1-x})TiO_3$ system. Finally, $\{\eta_{loc}\}$ characterizes the strain resulting from the difference in ionic size between Ba and Sr atoms, which is relatively large ($\simeq 2\%$). Such latter term is practically computed (when using the Voigt notation) at the B-site i as

$$\eta_{loc,1}(i) = \eta_{loc,2}(i) = \eta_{loc,3}(i) = \frac{\Delta a}{8a}\sum_j \sigma_j,$$

$$\eta_{loc,4}(i) = \eta_{loc,5}(i) = \eta_{loc,6}(i) = 0, \quad (2)$$

where Δa is the 0 K difference between the lattice constant of cubic $BaTiO_3$ and the a cubic lattice parameter of the virtual VCA-$\langle Ba_{0.5}Sr_{0.5}\rangle TiO_3$ material, and where the sum over j runs over the eight A nearest neighbors of the B-site i. It is important to realize that $\{\eta_{loc}\}$ has been omitted in the previous developments of effective Hamiltonian approaches for Pb-based solid solutions,[9–13] mostly because properties of such systems can be well mimicked around a fixed composition without the need of incorporating $\{\eta_{loc}\}$. Such strain allows here the unit cells to expand (respectively, contract) around Ba (respectively, Sr) atoms for a given composition since Δa is positive. It also allows the lattice constant to increase when increasing the overall Ba composition, and is the key quantity to be able to predict properties of BST materials *for any concentration*.

For E_{ave}, we use the analytical expression proposed in Ref. 23 for *simple* ABO_3 systems. E_{ave} thus consists of five parts: a local-mode self-energy (that includes quadratic and quartic terms in $\mathbf{u}_i$), a long-range dipole-dipole interaction, a short-range interaction between soft modes (which is quadratic in $\mathbf{u}_i$), an elastic energy (which is quadratic in η_H and η_I), and an interaction between the local modes and strain (which is linear in strain and quadratic in local modes).[23]

TABLE I. LDA-derived expansion parameters (in atomic units) of E_{ave} following the notations of Ref. 23.

Parameter	Value
a	7.371
κ_2	+0.0647
α	+0.2808
γ	−0.4128
j_1	−0.02402
j_2	+0.04444
j_3	+0.00841
j_4	−0.00474
j_5	+0.00707
j_6	+0.00151
j_7	+0.00075
B_{11}	+4.776
B_{12}	+1.610
B_{44}	+1.725
B_{1xx}	−1.973
B_{1yy}	−0.041
B_{4yz}	−0.059
Z^*	9.66
ϵ_∞	5.21

For E_{loc}, we propose the following expression:

$$E_{loc}(\{\mathbf{u}_i\},\{\eta_I\},\{\sigma_j\},\{\eta_{loc}\}) = \sum_{ij}[Q_{j,i}\sigma_j\mathbf{e}_{ji}\cdot\mathbf{u}_i + R_{j,i}\sigma_j\mathbf{f}_{ji}\cdot\mathbf{v}_i] + \frac{1}{2}\sum_i\sum_{l,\alpha,\beta} B_{l\alpha\beta}\eta_{loc,l}(i)u_{i,\alpha}u_{i,\beta} \quad (3)$$

where the sums over i and j run over unit cells and mixed sublattice sites, respectively, and where α and β denote the Cartesian components of the local modes centered on the cell i. As in Refs. 9–13, the $Q_{j,i}$ and $R_{j,i}$ parameters quantify how the alloy configuration perturbs the local modes and the $\{\eta_I\}$ inhomogeneous strain tensor of the VCA-$\langle Ba_{0.5}Sr_{0.5}\rangle TiO_3$ system, respectively. (Note that $\{\mathbf{v}_i\}$ are the A-centered dimensionless local displacements which are related to the inhomogeneous strain variables inside each cell).[23] $\mathbf{e}_{ji}$ is a unit vector joining the A site j to the B center of the soft-mode vector $\mathbf{u}_i$, and $\mathbf{f}_{ji}$ is a unit vector joining the A site j to the A origin of the displacement $\mathbf{v}_i$. Practically, we included contributions over the first-neighbor shell for $Q_{j,i}$ and up to the third neighbors for $R_{j,i}$. The last term of Eq. (3) is an original alloy contribution, in the sense that it was not included in the alloy effective Hamiltonians of Refs. 9–13. It characterizes the interactions between the $\{\eta_{loc}\}$ strain (arising from the relatively large size difference between Ba and Sr ions) and the local modes.

All the parameters of Eqs. (1)–(3) are derived from first-principles calculations performed on relatively small cells (i.e., up to 40 atoms), and are listed in Tables I and II. Note that comparing this Table II with the Table II of Ref. 10 indicates that the $Q_{j,i}$ and $R_{j,i}$ parameters of BST are one order of magnitude *smaller* than those of $Pb(Zr_{0.5}Ti_{0.5})O_3$, implying that the most important alloy effects in BST materials are those related to $\{\eta_{loc}\}$ and thus involving the last term of Eq. (3). (We further numerically confirmed this fact by checking that turning off the $Q_{j,i}$ and $R_{j,i}$ parameters, unlike switching off $\{\eta_{loc}\}$, does *not* significantly change the results in BST systems.) The first-principles method used in the present study is the plane-wave ultrasoft-pseudopotential method[24] within the local-density approximation[25] (LDA). The VCA approach adopted averages the Ba and Sr pseudopotentials, and is the one of Ref. 21.

TABLE II. LDA-derived expansion parameters of E_{loc} (in atomic units).

Parameter	Value
$\Delta a/a$	0.01087
Q_1	−0.00021
R_1	−0.00129
R_2	−0.00048
R_3	−0.00005

Once our effective Hamiltonian is fully specified, the total energy of Eq. (1) is used in Monte Carlo simulations, using the Metropolis algorithm,[26] to compute *finite-temperature* properties of systems containing Ba, Sr, Ti, and O atoms. Note that, as in Ref. 23, we perform these simulations under a negative external pressure to correct for the LDA underestimation of the lattice parameter. Here, this pressure (that couples with the homogeneous strain tensor) is chosen to be −5.2 GPa. The $\{\sigma_j\}$ variables are kept fixed during the Monte Carlo simulations. According to Eq. (2), this implies that $\{\eta_{loc}\}$ is also frozen during these simulations. The outputs of the Monte Carlo procedure are the local mode vectors **u** (directly related to the electrical polarization), and the homogeneous strain tensor η_H. Typically, up to 10^5 Monte Carlo sweeps are first performed to equilibrate the system, and then 10^5 sweeps are used to get the various statistical averages. The temperature is decreased in small steps.

III. RESULTS

A. Disordered solid solutions

We first investigate a disordered $(Ba_{0.5}Sr_{0.5})TiO_3$ alloy within the first-principles-based approach detailed in the previous section with the LDA-derived parameters given in Tables I and II. We use a $14\times14\times14$ supercell (13720 atoms) to get converged results and randomly choose the $\{\sigma_j\}$ variables to mimic such alloy. Four phases are numerically found in this system when decreasing the temperature: paraelectric cubic, ferroelectric tetragonal, ferroelectric orthorhombic, and ferroelectric rhombohedral. Such phase transition sequence is exactly the experimental one for this specific combination of Ba and Sr compositions.[17,18] On the other hand, we found that our predicted transition temperatures are lower by $\simeq$150 K from the measured values.[17,18] This underestimation by the effective Hamiltonian approach has already been observed in simple perovskite systems,[23,27,28] and may be due to higher-order terms missing in the effective Hamiltonian expansion and/or the neglect of phonon modes that are neither associated with the $\{\mathbf{u}_i\}$ local modes nor the strain tensors appearing in Eq. (1).[29] To correct it, we follow the "recipe" given in Ref. 30 and that has brought the theoretical dielectric constant of $KTaO_3$ in very good agreement with its experimental counterpart, including the (challenging to mimic) temperature width and magnitude of the quantum-induced low-temperature dielectric plateau. In other words, we decided to vary the κ_2 parameter that appears in the local-mode self-energy. Such parameter has been practically decreased by 20% in magnitude in order that the theoretical Curie temperature closely matches the corresponding measured values of disordered $(Ba_{0.5}Sr_{0.5})TiO_3$ alloy, that vary between[18] 220 K and[17] 250 K in the literature.

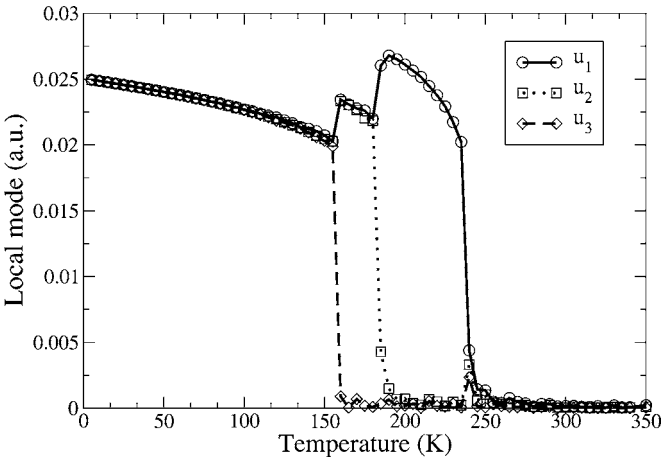

FIG. 1. Largest, middle, and smallest average Cartesian coordinates u_1, u_2, and u_3 of the local-mode vector as a function of temperature in disordered single crystals of $(Ba_{0.5}Sr_{0.5})TiO_3$, using the numerical approach described in Eqs. (1)–(3) with κ_2 having been reduced by 20% from its LDA-derived value.

Figure 1 shows the largest, middle, and smallest Cartesian coordinates (u_1, u_2, and u_3) of the supercell average of the local mode vectors in disordered $(Ba_{0.5}Sr_{0.5})TiO_3$ as a function of the temperature, as predicted by the approach described by Eqs. (1)–(3) but in which we now used this empirically found κ_2 (while keeping the other parameters equal to their LDA values). This figure indicates (1) a transition from a cubic paraelectric phase (in which each coordinate is close to zero) to a tetragonal ferroelectric phase (in which u_1 drastically increases while u_2 and u_3 remain nearly null) at 235 K±5 K; (2) a tetragonal-to-orthorhombic transition, for which u_2 now increases and becomes equal to u_1, at 180 K±5 K; and (3) an orthorhombic-to-rhombohedral transition, where all the coordinates are nonzero and equal to each other, at 155 K±5 K. Interestingly, while κ_2 was only adjusted to match the experimental Curie temperature, the 20% decrease of this parameter with respect to its LDA value also leads to an excellent agreement with measurement for the two lowest transitions in disordered $(Ba_{0.5}Sr_{0.5})TiO_3$ alloy. As a matter of fact, in this solid solution, the tetragonal-to-orthorhombic transition has been observed to occur around[17,18] 180 K while measured values for the temperature of the transition between the orthorhombic and rhombohedral phases are reported to be around 140 K.[17,18]

We now investigate the accuracy of the presently proposed method, with the adjusted κ_2 parameter, to reproduce the *whole* temperature-composition phase diagram of disordered $(Ba_xSr_{1-x})TiO_3$ solid solutions. Our predictions for $12\times12\times12$ supercells are reported in Fig. 2 along with the experimental data of Refs. 17 and 18. One can notice that the agreement between theory and measurement is overall very good for Ba compositions larger than 25%, at the sole exception of the orthorhombic-to-rhombohedral transition tem-

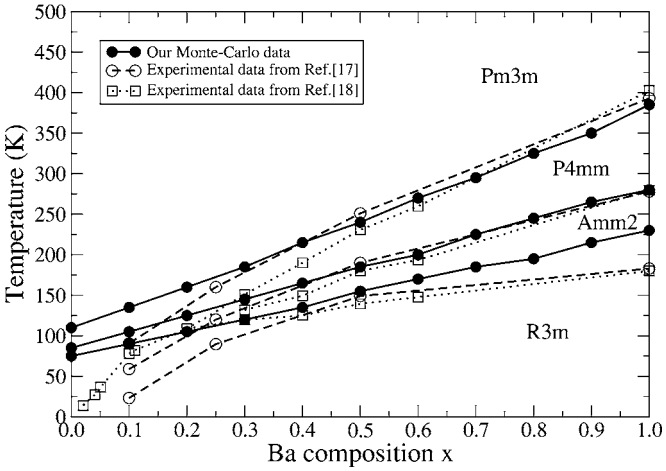

FIG. 2. Phase diagram of disordered $(Ba_xSr_{1-x})TiO_3$ solid solutions. Filled symbols show our predictions using the numerical approach described in Eqs. (1)–(3) with κ_2 having been reduced by 20% from its LDA-derived value. Open dots and squares symbols represent the experimental data of Refs. 17 and 18, respectively. Lines are guides for the eyes. The uncertainty on the theoretical transition temperatures is estimated to be around 5 K.

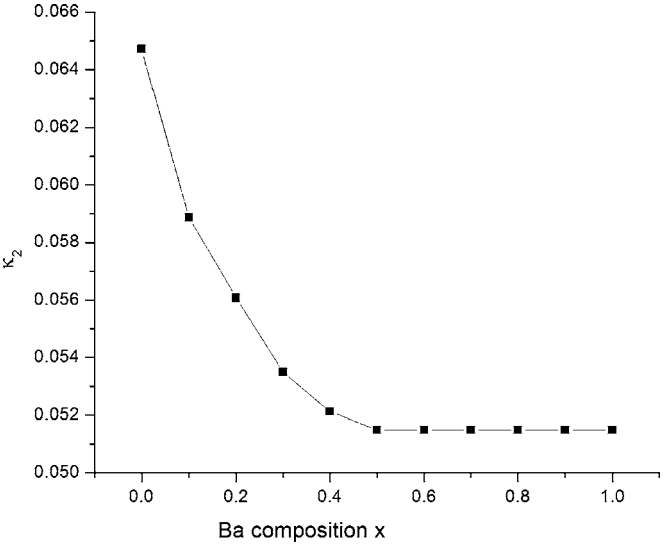

FIG. 3. Composition-dependency of the κ_2 parameter leading to theoretical Curie temperature matching the experimental values for the whole composition range.

perature that the theory slightly overestimates for the largest x concentrations. For instance, for pure $BaTiO_3$, our model predicts critical temperatures of 385±5 K, 280±5 K, and 230±5 K, for the cubic-to-tetragonal, tetragonal-to-orthorhombic, and orthorhombic-to-rhombohedral transitions, respectively, to be compared with the corresponding experimental values of ≃400 K, 280 K, and 180 K. For Ba compositions larger than 25%, our model thus appears to be more accurate than the shell model of Ref. 3, for which the Curie temperature is always underestimated by at least 50 K. However, one has to realize that this shell model is purely *ab initio*, while we had to adjust one parameter with respect to its first-principles value, in order to obtain a Curie temperature that agrees with experiment for the sole composition of $x=0.5$. Note also that our model predicts the right phase *for any composition at room temperature*, i.e., ferroelectric tetragonal for x larger than ≃70% and paraelectric cubic for lower Ba concentrations. On the other hand, Fig. 2 also indicates that the results of our simulations deviate more and more from the measurement *at low temperature* when decreasing the Ba composition below 25%. For instance, our calculations still yield, below ≃110 K, the full transition sequence cubic-ferroelectric tetragonal-ferroelectric orthorhombic-ferroelectric rhombohedral in pure $SrTiO_3$ while this simple system is known to *not* exhibit ferroelectricity down to 0 K (except if substituting O^{16} by^{31} O^{18}) but rather antiferrodistortive motions. In fact, this disagreement is actually expected in the sense that the reduction/suppression of ferroelectricity in $(Ba_xSr_{1-x})TiO_3$ solid solutions with large Sr content is due to two effects that we did *not* include in our present model, namely quantum effects and the coupling between ferroelectricity and antiferrodistortive motions (that are both known to be important at low temperature in pure[32,33] $SrTiO_3$). In other words, using path-integral quantum Monte Carlo simulations[30,32,34,35] (rather than classical ones as we do here) to mimic zero-point phonon vibrations, and extending our present approach to incorporate antiferrodistortive motions and their couplings (as in Ref. 33), should most certainly bring theoretical predictions in better agreement with measurement for low temperature at large Sr compositions. (Such extensions may constitute the basis of a future work.) This fact is clearly corroborated by Fig. 3 that displays the numerically-found compositional evolution of the κ_2 parameter that yields Curie temperatures predicted by the method described in Eqs. (1)–(3) matching the experimental ones for the *whole* composition range. One can clearly see that κ_2 sharply increases when decreasing the Ba content below 25%, which characterizes an increased (Sr induced) suppression of ferroelectricity.

B. Epitaxial superlattices

Having tested our effective Hamiltonian model for stress-free disordered $(Ba_xSr_{1-x})TiO_3$ solid solutions, we now apply it to know if it also yields accurate results for various $(BaTiO_3)_m/(SrTiO_3)_n$ superlattices grown along the z axis (chosen to be along the pseudocubic [001] direction) and constrained to have the in-plane lattice constant of pure (paraelectric) $SrTiO_3$. We thus mimic superlattices epitaxially grown on a $SrTiO_3$ substrate. One first has to realize that, because of Eq. (2), the lattice constant along the x and y axes of a system having an overall x Ba composition are related (in Voigt notation) to $\eta_{H,1}+\frac{\Delta a}{a}(2x-1)$ and $\eta_{H,2}+\frac{\Delta a}{a}(2x-1)$, respectively. As a result, in order to mimic a system epitaxially grown on a $SrTiO_3$ substrate, we impose these two latter sums to be equal to the 0 K relative lattice mismatch between cubic $SrTiO_3$ and cubic VCA-$\langle Ba_{0.5}Sr_{0.5}\rangle TiO_3$. (Note that the origin of strain is defined with respect to 0 K cubic VCA-$\langle Ba_{0.5}Sr_{0.5}\rangle TiO_3$ in our approach.) We also impose $\eta_{H,6}$ to vanish and allow the other components of the homogeneous strain tensor to relax during the Monte Carlo simulations in order to fully simulate an epitaxial growth along [001].[36–39]

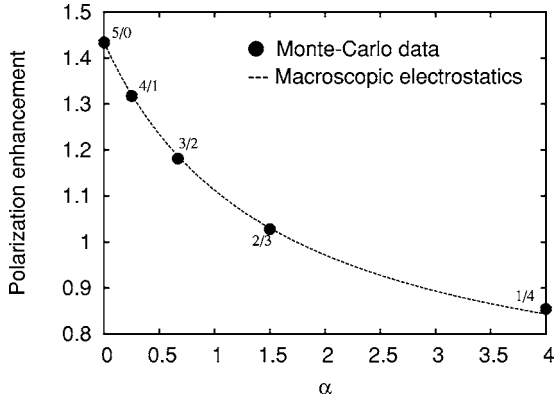

FIG. 4. Dependency of the polarization along the [001] direction on the ratio of the number of $SrTiO_3$ layers over the number of $BaTiO_3$ layers in epitaxially-strained $BaTiO_3/SrTiO_3$ superlattices at 5 K. The filled symbols represent our predictions using the numerical approach described in Eqs. (1)–(3) with κ_2 having been reduced by 20% from its LDA-derived value. The dotted line displays the best fit of our results to Eq. (4), which is derived from simple macroscopic electrostatics.

Here, we focus on the low-temperature properties of the epitaxial superlattices studied in Ref. 19 by direct first-principles techniques, that are 5/0 (pure $BaTiO_3$), 4/1, 3/2, 2/3, and 1/4 when using the m/n notation for describing the m and n periods of the $BaTiO_3$ and $SrTiO_3$ layers, respectively. In particular, we are interested to check if our method is able to reproduce a remarkable result of Ref. 19, namely that the polarization in short-period $(BaTiO_3)_m/(SrTiO_3)_n$ superlattices can be predicted by simple macroscopic electrostatic arguments involving the short-circuit boundary conditions experienced by the superlattices and the equality between the electric displacements of the $BaTiO_3$ and $SrTiO_3$ layers.

Figure 4 reports our predicted P/P_0 ratio (where P and P_0 are the polarizations along the [001] direction in the studied superlattice and in tetragonal $BaTiO_3$ bulk, respectively) *versus* the $\alpha=n/m$ ratio, at 5 K and when using the approach described by Eqs. (1)–(3), in which κ_2 has been decreased by 20% from its LDA value, for $1\times1\times5$ supercells. Figure 4 also indicates that these numerical data can be extremely well fitted by the electrostatic-derived formula

$$P = \frac{P_{5/0} + \alpha\beta P_{0/5}}{1 + \alpha\beta}, \tag{4}$$

when using $\beta=0.647$ and where $P_{5/0}$ and $P_{0/5}$ are the polarizations along the [001] direction in strained $BaTiO_3$ and in pure $SrTiO_3$, respectively, as predicted by our method.[40] This β parameter, which corresponds to the ratio between the dielectric constant of $BaTiO_3$ and $SrTiO_3$ in the general electrostatic model used to derive Eq. (4), is rather close to the one found by Neaton and Rabe, that is 0.423.[19] Note that we numerically found that this β parameter is slightly dependent on the lattice constant used for pure $SrTiO_3$ or other technical details, which probably explains the slight difference in β between our results and that of Ref. 19. For instance, switching off the pressure of −5.2 GPa in our simulations (such pressure was introduced to overcome the LDA underestimation of the lattice constant) results in $\beta\simeq0.5$. In any case, we have proven that our relatively simple method is also able to reproduce the fact that the properties of short-period $(BaTiO_3)_m/(SrTiO_3)_n$ superlattices can be understood by simple macroscopic electrostatics argument,[19] without having to impose any macroscopic electrostatic equation in our modeling and despite the fact that the sole dielectric constant appearing among the effective Hamiltonian parameters is the electronic one associated with VCA-$\langle Ba_{0.5}Sr_{0.5}\rangle TiO_3$ (see Tables I and II).

IV. CONCLUSIONS

In summary, we have developed an original alloy effective Hamiltonian approach to investigate finite-temperature properties of perovskite systems containing Ba, Ti, Sr, and O atoms. When allowing one single parameter to deviate from its LDA-derived value, this approach gives predictions that (1) are overall in good qualitative *and* quantitative agreement with experiments for the composition-temperature phase diagram of disordered $(Ba_xSr_{1-x})TiO_3$ solid solutions; and (2) reproduce subtle features of $BaTiO_3/SrTiO_3$ superlattices previously found by direct first-principles calculations.[19] The use of this numerical scheme thus may allow, in the future, the investigation and microscopic understanding of challenging problems in BST-based materials. Examples of such problems are the effect of short-range and long-range atomic order[41,42] on the finite-temperature properties of BST solid solutions, and the unusual dipole patterns and dielectric responses found in some $BaTiO_3/SrTiO_3$ superlattices (see, e.g, Refs. 43–47 and references therein). One can also imagine using this scheme within an inverse method[48] to determine the overall composition and atomic arrangement leading to optimal piezoelectric and dielectric properties in BST compounds. Finally, the proposed method can be generalized, without too much effort and following Refs. 36 and 49–53 to study low-dimensional BST systems—such as thin films, wires, and dots—that are of large current interest.

ACKNOWLEDGMENTS

This work is supported by ONR Grants No. N00014-01-1-0365, No. N00014-04-1-0413, and No. N00014-01-1-0600, by NSF Grants No. DMR-0404335 and No. DMR-9983678, and by DOE Grant No. DE-FG02-05ER46188. Some computations were made possible thanks to the Major Research Instrumentation Grant No. 0421099 from the National Science Foundation, and by a grant of HPC resources from the Arctic Region Supercomputing Center at the University of Alaska Fairbanks as part of the Department of Defense High Performance Computing Modernization Program. We thank J. M. Kiat, Igor Kornev, and Sergey Prosandeev for useful discussions.

[1] K. Uchino, *Piezoelectric Actuators and Ultrasonic Motors* (Kluwer Academic Publishers, Boston, 1996).
[2] M. A. Akbas and P. K. Davies, J. Am. Ceram. Soc. **81**, 670 (1998).
[3] S. Tinte, M. G. Stachiotto, S. R. Phillpot, M. Sepliarsky, D. Wolf, and R. L. Migoni, J. Phys.: Condens. Matter **16**, 3495 (2004).
[4] M. Sepliarsky, S. R. Phillpot, M. G. Stachiotti, and R. L. Migoni, J. Appl. Phys. **91**, 3165 (2002).
[5] M. Sepliarsky, S. R. Phillpot, D. Wolf, M. G. Stachiotti, and R. L. Migoni, J. Appl. Phys. **90**, 4509 (2001).
[6] S. R. Phillpot, M. Sepliarsky, S. K. Streiffer, M. G. Stachiotti, and R. L. Migoni, AIP Conf. Proc. **626**, 160 (2002).
[7] B. Noheda, D. E. Cox, G. Shirane, J. A. Gonzalo, L. E. Cross, and S.-E. Park, Appl. Phys. Lett. **74**, 2059 (1999).
[8] I. Grinberg, V. R. Cooper, and A. M. Rappe, Nature (London) **419**, 909 (2002).
[9] L. Bellaiche, A. García, and D. Vanderbilt, Phys. Rev. Lett. **84**, 5427 (2000).
[10] L. Bellaiche, A. García, and D. Vanderbilt, Ferroelectrics **266**, 41 (2002).
[11] R. Hemphill, L. Bellaiche, A. García, and D. Vanderbilt, Appl. Phys. Lett. **77**, 3642 (2000).
[12] R. Haumont, B. Dkhil, J. M. Kiat, A. Al-Barakaty, and L. Bellaiche, Phys. Rev. B **68**, 014114 (2003).
[13] A. Al-Barakaty and L. Bellaiche, Appl. Phys. Lett. **81**, 2442 (2002).
[14] E. Cockayne, B. Burton, and L. Bellaiche, *Fundamental Physics of Ferroelectrics 2001: 11th Williamsburg Ferroelectric Workshop*, edited by H. Krakauer (AIP, Melville, New York, 2001), p. 191.
[15] K. Leung, E. Cockayne, and A. F. Wright, Phys. Rev. B **65**, 214111 (2002).
[16] K. Abe and S. Komatsu, J. Appl. Phys. **77**, 6461 (1995).
[17] C. Menoret, J. M. Kiat, B. Dkhil, M. Dunlop, H. Dammak, and O. Hernandez, Phys. Rev. B **65**, 224104 (2002).
[18] V. V. Lemanov, E. P. Smirnova, P. P. Syrnikov, and E. A. Tarakanov, Phys. Rev. B **54**, 3151 (1996).
[19] J. B. Neaton and K. M. Rabe, Appl. Phys. Lett. **82**, 1586 (2003).
[20] L. Nordheim, Ann. Phys. **9**, 607 (1931).
[21] L. Bellaiche and D. Vanderbilt, Phys. Rev. B **61**, 7877 (2000).
[22] N. J. Ramer and A. M. Rappe, J. Phys. Chem. Solids **61**, 317 (2000).
[23] W. Zhong, D. Vanderbilt, and K. M. Rabe, Phys. Rev. Lett. **73**, 1861 (1994); Phys. Rev. B **52**, 6301 (1995).
[24] D. Vanderbilt, Phys. Rev. B **41**, R7892 (1990).
[25] P. Hohenberg and W. Kohn, Phys. Rev. **136**, B864 (1964); W. Kohn and L. J. Sham, *ibid.* **140**, A1133 (1965).
[26] N. Metropolis, A. W. Rosenbluth, M. N. Rosenbluth, A. H. Teller, and E. Teller, J. Chem. Phys. **21**, 1087 (1953).
[27] U. Waghmare and K. M. Rabe, Phys. Rev. B **55**, 6161 (1997).
[28] H. Krakauer, R. Yu, C.-Z. Wang, and C. LaSota, Ferroelectrics **206-207**, 133 (1998).
[29] S. Tinte, J. Iniguez, K. M. Rabe, and D. Vanderbilt, Phys. Rev. B **67**, 064106 (2003).
[30] A. R. Akbarzadeh, L. Bellaiche, Kevin Leung, Jorge Íñiguez, and David Vanderbilt, Phys. Rev. B **70**, 054103 (2004).
[31] M. Itoh, R. Wang, Y. Inaguma, T. Yamaguchi, Y-J. Shan, and T. Nakamura, Phys. Rev. Lett. **82**, 3540 (1999).
[32] W. Zhong and D. Vanderbilt, Phys. Rev. B **53**, 5047 (1996).
[33] W. Zhong and D. Vanderbilt, Phys. Rev. Lett. **74**, 2587 (1995).
[34] D. M. Ceperley, Rev. Mod. Phys. **67**, 279 (1995).
[35] J. Íñiguez and D. Vanderbilt, Phys. Rev. Lett. **89**, 115503-1 (2002).
[36] I. Kornev, H. Fu, and L. Bellaiche, Phys. Rev. Lett. **93**, 196104 (2004).
[37] N. A. Pertsev, V. G. Kukhar, H. Kohlstedt, and R. Waser, Phys. Rev. B **67**, 054107 (2003).
[38] O. Dieguez, S. Tinte, A. Antons, C. Bungaro, J. B. Neaton, K. M. Rabe, and D. Vanderbilt, Phys. Rev. B **69**, 212101 (2004).
[39] B.-K. Lai, I. A. Kornev, L. Bellaiche, and G. J. Salamo, Appl. Phys. Lett. **86**, 132904 (2005).
[40] Note that our Eq. (4) slightly differs from the Eq. (2) of Ref. 19 by the additional term $\alpha\beta P_{0/5}$ in the numerator. This difference is caused by the fact that, unlike in the present case (see Fig. 2), Ref. 19 found that $SrTiO_3$ is paraelectric cubic (and thus leads to a vanishing $P_{0/5}$), as a result of the $\simeq 2\%$ LDA underestimation of the lattice constant.[19]
[41] A. M. George, J. Íñiguez, and L. Bellaiche, Phys. Rev. Lett. **91**, 045504 (2003).
[42] A. M. George, J. Íñiguez, and L. Bellaiche, Nature (London) **413**, 54 (2001).
[43] L. Kim, D. Jung, J. Kim, Y. S. Kim, and J. Lee, Appl. Phys. Lett. **82**, 2118 (2003).
[44] A. Q. Jiang, J. F. Scott, H. Lu, and Z. Chen, Appl. Phys. Lett. **93**, 1180 (2003).
[45] H. Tabata, H. Tanaka, and T. Kawai, Appl. Phys. Lett. **65**, 1970 (1994).
[46] K. Johnston, X. Huang, J. B. Neaton, and K. M. Rabe, Phys. Rev. B **71**, 100103(R) (2005).
[47] A. L. Roytburd, S. Zhong, and S. P. Alpay, Appl. Phys. Lett. **87**, 92902 (2005).
[48] J. Íñiguez and L. Bellaiche, Phys. Rev. Lett. **87**, 095503 (2001).
[49] E. Almahmoud, Y. Navtsenya, I. Kornev, H. Fu, and L. Bellaiche, Phys. Rev. B **70**, 220102(R) (2004).
[50] I. Ponomareva, I. I. Naumov, I. Kornev, H. Fu, and L. Bellaiche, Phys. Rev. B **72**, 140102(R) (2005).
[51] I. Ponomareva, I. I. Naumov, and L. Bellaiche, Phys. Rev. B **72**, 214118 (2005).
[52] I. I. Naumov, L. Bellaiche, and H. Fu, Nature (London) **432**, 737 (2004).
[53] H. Fu and L. Bellaiche, Phys. Rev. Lett. **91**, 257601 (2003).